Spectroscopic studies of polaronic and bipolaronic species in n-doped poly(paraphenylenevinylene)

I. Orion, J. P. Buisson, and S. Lefrant

Laboratoire de Physique Cristalline, Institut des Matériaux de Nantes, 2 rue de la Houssinière, Boîte Postale 32229,
44322 Nantes Cedex 3, France

In this paper, we present a detailed study of the vibrational properties of neutral and n-doped polyparaphenylene-vinylene (PPV). Resonance Raman scattering and infrared-absorption results are analyzed and interpreted by the use of dynamical calculations based on a valence force-field model. Experimental data include those obtained from related oligomers, i.e., trans-stilbene and distyrylbenzene with the assumption of similar geometry parameters. Force constants are optimized according to assignments of Raman and ir vibrational bands of the series of compounds. In the case of sodium-doped PPV, new Raman bands are observed showing different resonance behaviors. These new features are investigated as a function of the doping level, leading to the conclusion that polarons and bipolarons of short lengths coexist in thermodynamical equilibrium. Doping-induced bands are interpreted in terms of changes in carbon-carbon force constants. Such modifications in the electronic distribution agree well with the quinoid character expected upon doping on the polymeric chains. [S0163-1829(98)03811-9]

I. INTRODUCTION

Conjugated polymers have attracted a great deal of interest from scientists over the last two decades due to their conducting state occurring after doping with electron donors or acceptors.[1-3] However, considerable attention has also been paid to their neutral state because these materials exhibit interesting electronic properties as semiconductors with energy gaps ranging from approximately 1.5 eV to 3–4 eV. In addition, compared to low molecular weight compounds, one can gain from other characteristics such as their high mechanical strength, high melting point, easy processability, etc. As a matter of fact, organic polymers are known to be good candidates for applications in different domains, especially optoelectronics or photonics, in the fabrication of nonlinear optical devices (NLO's) for example, since NLO properties can be expected due to readily polarizable π-conjugated electrons. Due to the development of soluble precursors, these polymers can be easily processed and therefore the fabrication of electroluminescent and photovoltaic devices has been achieved. Polyphenylene-vinylene for example (hereafter referred to as PPV) is considered as a prototype of nondegenerate ground state polymers [Fig. 1(a)], which in turn exhibits good stability and high conductivity after doping. Moreover, a large number of substituted derivatives have been successfully prepared in the purpose of monitoring both their electronic and optical properties. This has led to the development of efficient light emitting diodes (LED's) at different emission wavelengths. Demonstrated by J. H. Burroughes *et al.*[4] in 1990, considerable improvements have been made since their discovery. Applications of such compounds in photonics has been reviewed recently[5] and the fabrication of so-called polymeric optochips described.[6,7]

In the case of PPV and substituted derivatives, the main objective of scientists is still to optimize these polymers in the purpose of increasing the time life of devices such as LED's. Therefore, a complete control of the synthesis is needed in terms of conjugated length, chemical stability, defects, etc.

In a fundamental point of view, the understanding of the physical properties of conjugated polymers involved in transport or optical phenomena requires a detailed study of their electronic excitations. Contrarily to usual inorganic semiconductors, several differences can be stressed out. The conducting state of such compounds is achieved after n or p doping, which means a large incorporation of counter ions (several percents in atomic ratios). Electrical properties are therefore issued from the presence of a high concentration of extrinsic charge carriers. Due to a strong electron-lattice coupling, these charge carriers present a polaronic character. This interaction leads to a trapping of the added charges which induces a local distortion in the polymeric backbone. Polaronic or bipolaronic excitations are thus expected and can be studied in conjugated polymers by using several techniques, e.g.,
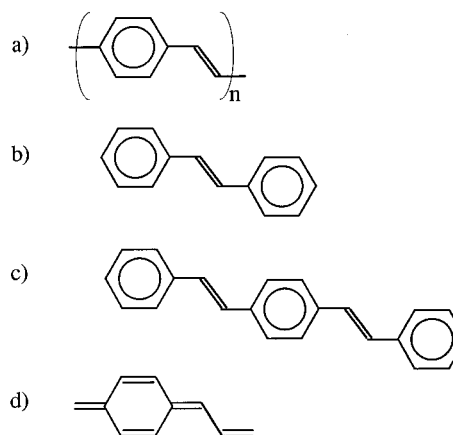

FIG. 1. Molecular structure of (a) poly(p-phenylenevinylene) (PPV) repeat unit; (b) trans-stilbene (TSB); (c) t,t-distyrylbenzene (DSB); (d) schematic diagram of the quinoid form.

optical and magnetic spectroscopies, conductivity measurements, etc.

The purpose of this paper is to describe the modifications encountered by the conjugated structure of PPV between its neutral and conducting states. In this respect, vibrational spectroscopies, such as resonance Raman scattering (RRS) and infrared absorption, are specially appropriate to probe intrachain modifications involving both polymeric structure and electronic distribution along the chain. Theoretical calculations issued from band structure[8] or modified neglect of differential overlap (MNDO) (Ref. 9) methods have predicted a ''quinoid'' character for polarons and bipolarons in PPV [Fig. 1(d)]. Such charged defects are supposed to extend over approximately 3 to 5 polymer units, in rough agreement with experimental estimations of polarons and bipolarons lengths obtained by comparison with anionic or cationic model compounds.[10,11] Our purpose is to discuss this prediction with a different point of view, namely, from the modelization of Raman and infrared spectra since, as said before, vibrational spectroscopies can be used to investigate chain changes upon doping. From Raman-scattering and infrared-absorption observations, the polymer structure can be quantitatively described in the frame of a valence force field model using the formalism of the Fourier dynamic matrix. Changes related to the presence of polaronic or bipolaronic defects can then be interpreted in terms of a perturbation of the pristine sample, which will be discussed according to the above picture.

In Sec. II of this paper, we report the experimental details while in Sec. III, we describe both the experimental results and the valence force-field model established for neutral PPV, which contains several refinements compared to previous works.[12] The optimization process has been carried out via a combined study of oligomers, in particular trans-stilbene (TSB) and distyril-benzene (DSB) shown in Figs. 1(b) and 1(c). Such a methodology ensures a correct assignment of the observed vibrational bands that can be followed from one compound to the other along the series. A further advantage is to determine an optimum set of force constants common to all compounds, established on a large number of experimental frequencies. A previously determined benzene valence force field[13] has been used for the parameters related to aromatic rings. Hence our work is a direct continuation of reliable vibrational studies on aromatic compounds.

Both n- or p-type doping induce modifications in experimental vibrational spectra of conducting polymers. Different spectral changes are observed depending on the state of charge, whether electrons are added or removed from the polymer backbone. Indeed, there is no reason to expect that the electronic polarizability involved in Raman scattering undergoes the same modifications in these two cases. We have devoted Sec. IV of this paper to n-type doping illustrated by sodium-doped PPV. The experimental investigation has been carried out using RRS in order to discriminate between several coexisting species. Results presented in this paper complete those published in Ref. 14 and provide additional information to the work of Sakamoto and co-workers.[11] Spectral changes are then interpreted via a vibrational analysis in terms of modifications in the valence force field, and further, in terms of structural relaxation along the polaronic or bipolaronic segments. In order to compare with theoretical
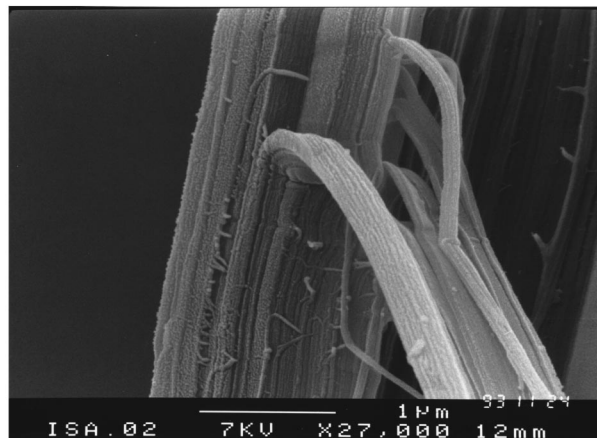

FIG. 2. Scanning electron microscope picture of a stretched-oriented PPV film.

predictions, use is made of a previously determined semi-empirical relation between the F_{C-C} force constants and the corresponding C-C bond lengths[15] denoted r_{cc}. This relationship shows a linear dependence in $1/r_{cc}^4$:

$$F_{C\text{-}C} \propto 1/r_{cc}^4. \tag{1}$$

II. EXPERIMENTAL DETAILS

A. Materials

PPV free-standing films with ca. 5 to 10 μm thickness were synthesized in our laboratory via the soluble polysulfonium precursor polymer route. Details on this process are widely described in the literature.[16,17] This method is known to yield high molecular weight polymer,[18] with high purity and significative conjugation length.[19] After purification by dialysis, a solution of poly(p-xylylidine tetrahydrothiophenium chloride) is cast into films by water evaporation under nitrogen atmosphere. Precursor films are then gradually annealed up to 300 °C under vacuum ($p \sim 10^{-6}$ Torr) for approximately 10 h. During this thermal treatment, the sulfonium lateral groups are eliminated, giving rise to the unsaturated vinylene linkage with a ''trans'' configuration. These changes can be characterized by the observation of a strong band at 966 cm^{-1} in ir spectra, corresponding to an out-of-plane vibration of the transvinylene intercycle.[20,21] The use of tetrahydrothiophenium leaving groups is known to avoid side reactions during the thermal conversion.[22] Elemental analysis indicates sulfur and chlorine contents less than 1%. Also, compared to other possible sulfonium moieties, tetrahydrothiophenium groups improve the cristallinity and the conjugation length. This has been confirmed by diffraction studies,[23] by the red shift of the absorption maxima in optical spectra[17,19] and by solid-state ^{13}C NMR showing no evidence for sp^3 hybridized carbon (not shown). Further, the precursor polymer route offers the possibility of obtaining oriented polymer: a rapid stretching of the precursor film while heating between 60 °C and 100 °C (Ref. 24) yields highly oriented PPV (Fig. 2) with draw ratios up to ≈ 10, on which the thermal elimination is completed as described

above. Oligomers were either purchased when available (TSB from Aldrich) and recrystallized, or supplied by other groups.

Sodium doping of PPV films has been performed either by vapor phase[25,26] or solution[27] techniques. In the former case, glass tubes containing PPV pieces and distilled sodium were sealed under vacuum ($\sim 10^{-6}$ torr), and heated at 200 °C for various durations (typically several hours) until samples get metalliclike colors. This out-of-equilibrium process leads to a nonuniform insertion of sodium, as one can observe through the gradation of colors. Pristine PPV films being orange, doped areas get first a grey luster, becoming successively blue-green, violet, and finally gold at the ultimate stage. On the other hand, doping in solution uses a reduction reaction with an organo-sodium salt in anhydrous tetrahydrofuran, which is carried on during several weeks until the thermodynamical equilibrium is reached.[27] Different doping levels can be obtained depending on the radical-anion system involved in this reaction. Sodium ratios are evaluated by acidimetry after alcaline extraction in methanol. In this way, PPV-Na samples with averaged sodium ratios of 20 ± 5 and $50 \pm 5\%$ mol Na/C_8H_6 have been prepared, corresponding, respectively, to blue and gold colors. It is noticeable that the highest obtained ratio is consistent with the 52% deduced by Chen and Winokur from diffraction studies on PPV-Na at maximum doping level[28] (with a vapor phase doping). Such a large dopant amount is also consistent with the ratio obtained when achieving the same treatment on polyacetylene[29] (15–16% mol Na/CH), once taking into account the respective lengths of 1.24 and 6.58 Å for C_2H_2 and C_8H_6 polymer units. Because of their extreme sensitivity against oxygen and water, sodium-doped films were kept in glass cells sealed under vacuum. We observed that Raman experiments performed on PPV-Na samples of given colors yield identical spectra whenever they were doped in vapor phase or in solution. Hence, the two above mentioned samples with determined ratios were used as references in order to calibrate other doping levels, using X fluorescence under scanning electron microscopy as a local analysis technique.

B. Apparatus and measurements

Resonance Raman-scattering experiments were performed with a Jobin-Yvon T64000 spectrometer equipped with a cooled charge-coupled device detector. Excitation lines were provided by Spectra Physics Ar^+ or Kr^+ lasers when operating in the visible or near uv range (from 350 to 676 nm). In the near ir, we used a Fourier transform (FT) Raman spectrometer Bruker RFS100 with a 1064 nm excitation issued from a Nd:YAG laser. Neutral compounds were investigated with relatively high laser power, from ~ 50 mW on the sample for excitations in the visible up to ~ 300 mW for the near ir excitation. A resolution of 2 cm^{-1} was used in order to discriminate with good accuracy overlapping Raman bands. Experiments were performed on PPV films either with 90° or backscattering geometries. In the case of doped samples, spectra were recorded only with a backscattering geometry under microscope providing the possibility to analyze inhomogeneously doped areas. The laser power was lowered (~ 30 mW for FT-Raman experiments) to avoid

thermal damages due to laser irradiation. The resolution was then increased to 8 cm^{-1} in order to get reasonable signal-to-noise ratios. Since Raman bands are significantly broadened in the conducting state, such a resolution turned out to be sufficient.

Infrared-absorption experiments in the 400–4000 cm^{-1} range were performed on a Nicolet 20 SXC Fourier transform infrared spectrometer with a deuterated triglycine sulfate detector, and those in the 50–650 cm^{-1} range on a Nicolet 20F spectrometer. A microbeam apparatus has been used to record polarized ir spectra in the 650–4000 cm^{-1} range. The resolution was 2 or 4 cm^{-1}. Samples in powder form were dispersed in KBr pellets, whereas free-standing films of PPV (5–10 μm thick) were directly investigated. All studies were carried out at room temperature.

III. DYNAMICAL STUDY OF THE NEUTRAL STATE

Our approach using model compounds aimed to describe the vibrational properties of PPV and its related oligomers in the frame of a common model. The structure of the different molecules has been defined with a same set of geometric parameters, bond lengths and angles corresponding to the internal coordinates used in the model. An optimization process performed on assigned vibrational frequencies leads to one set of force constants, which represents the valence force-field model for PPV series. Additional information issued from studies carried out in polarized light, calculated potential energy distribution and atomic displacements were also taken into account. The following section is devoted to the description of the different steps in building up the model.

A. Preliminaries

The molecular structure of TSB, DSB, and PPV is shown in Fig. 1 and internal coordinates are defined in Fig. 7 with DSB as the example. Their values have been chosen considering two kinds of information. Experimental data from x-ray-diffraction studies have been published for TSB only.[30,31] Consistent structural data for TSB and longer oligomers or PPV have also been obtained from *ab initio* or semiempirical calculations.[9,32–36] These methods lead to optimized geometric parameters almost independent on the size of the oligomer, and consistent with the values experimentally determined on TSB. Differences are less than 1%, except for the vinyl C=C bond length, for which the experimental value of 1.30 Å is 4% less than the calculated one. Bernstein[31] has stressed this point concerning this C=C length in TSB as being unusually short as compared to ethylenic bonds in other stilbenes (more commonly ~ 1.34 Å). Concerning the parameters used in our modelization, the following comments can be given in addition:

(i) The vinyl bond length is taken as $D = 1.35$ Å, as calculated for longer oligomers. The angles β, β', and β'' on the intercycle are taken from experimental values,[30,31] also in agreement with optimized geometries.

(ii) Aromatic rings are considered with the same geometry as the one used for the dynamical model of benzene.[13] In this work, as in previous studies on other series of aromatic compounds,[37–39] the benzene model is taken as a reference for the vibrations of phenyl groups.

(iii) The assumption of a mean planarity in the equilibrium configuration can be justified for these compounds in the solid state. The dihedral angle between the two cycles in TSB has been experimentally estimated to be less than 5° (Ref. 30). On the other hand, while theoretical calculations predict a twist angle of $25 \pm 5°$ for isolated molecules of TSB and longer oligomers,[32,40] the energetic barrier at 0° is flat enough to be compensated by the gain in compacity and in π orbitals overlapping in the solid state. This assumption is supported by the red shift (~ 0.15 eV) of the absorption threshold when going from solutions to crystalline compounds.[40] In regards to molecular vibrations, a planar equilibrium configuration leads to a separation between in-plane and out-of-plane vibration modes. In our model, only in-plane vibrations are considered, so that the set of internal coordinates excludes the twist angles since they do not contribute in the expression of such vibrations. The molecular geometry defined in this way provides a reference on which results of the PPV series modelization will be discussed.

In the planar all-trans configuration, PPV and related oligomers belong to the point group C_{2h}, and so, in-plane and out-of-plane normal modes are separated into symmetric and antisymmetric with respect to the molecular plane. The restriction to in-plane modes yields two degrees of freedom per atom. Inversion centers lying either on the vinyl group in TSB, on the central ring in DSB, or on both in PPV, lead to the exclusion rule between Raman-active modes (g modes) and ir active modes (u modes). The first step consists then in determining the number of the allowed modes for each compound. Therefore, if one restricts to in-plane vibrations, the following active vibrations can be listed:

TSB (26 atoms) $25\ A_g + 24\ B_u$ (including 6 A_g and 6 B_u modes coming from CH stretching vibrations),

DSB (40 atoms) $39\ A_g + 38\ B_u$ (including 9 A_g and 9 B_u modes coming from CH stretching vibrations),

PPV (14 atoms/unit cell) $14\ A_g + 12\ B_u$ (including 3 A_g and 3 B_u modes coming from CH stretching vibrations).

Notice that we have considered separately all modes issued from C-H vibrations. They are observed near 3000 cm^{-1} while other modes occur in a lower frequency range, up to 1800 cm^{-1} for aromatic compounds. In our calculations we have used the assignments of C-H stretching vibrations previously given by Meic and Güsten on TSB,[41] and we have focused our calculations on the lower frequency modes.

Active normal modes can also be listed in a parallel way by taking into account the contributions from the different molecular groups, namely, aromatic rings and vinyl groups. This procedure puts in evidence the filiations between vibrations along the series TSB-DSB-PPV. Results for in-plane and low-frequency modes are collected in Tables I and II.

B. Experimental results

1. Resonance Raman scattering

Raman spectra of TSB, DSB, and PPV recorded with the excitation wavelength $\lambda_L = 1064$ nm are shown in Fig. 3. They have been normalized on their strongest band observed at approximately 1590 cm^{-1}. With other excitation wavelengths the peak positions are unchanged within an accuracy of ± 2 cm^{-1}. This property is characteristic of oligomers with a defined length. In the case of the polymer for which a distribution of conjugation lengths is expected, the lack of frequency dispersion has already been noticed, and is consistent with other observations. First, energy gaps in compounds containing more than 10 C_8H_6 units[42,43] show almost no variation and are almost not sensitive to resonant Raman-scattering effects. Second, when comparing Raman spectra of TSB, DSB, and longer oligomers such as distyrylstylvene (DSV) that contains one extra C_8H_6 unit, experimental frequencies converge quickly to values observed in PPV. Thus, small variations of Raman frequencies as a function of the chain length in PPV is to be retained, in contrast to the case of polyacetylene.[44] On the other hand, some changes are observed in the relative intensities between the group of bands around 1170 cm^{-1} and the other around 1590 cm^{-1}. For example, the former group presents a maximum intensity when using an excitation wavelength $\lambda_L = 676$ nm, indicating clearly resonance effects.

A closer inspection of Fig. 3 shows that (i) the intensities of the bands at approximately 1000 and 1450 cm^{-1} vanish when going from TSB to PPV. This behavior is characteristic of vibrations localized on the external cycles. (ii) The DSB spectrum appears as a juxtaposition of the Raman spectra of TSB and PPV, as a consequence of the contributions from external and internal cycles, respectively (see Table I). (iii) In the high-frequency range, the intensity ratio between bands at 1546–1571 cm^{-1} and 1625–1638 cm^{-1} increases as a function of the conjugation length. This effect can also be followed during the conversion process, yielding a qualitative criterium for the conjugation extension in PPV samples.[45]

2. Infrared absorption

Infrared spectra of TSB, DSB, and PPV shown in Fig. 4 present a large number of bands, the strongest corresponding to out-of-plane modes, the induced dipolar moments being particularly strong. As noticed in Sec. II of this paper, the band at 966 cm^{-1} in PPV is characteristic of an out-of-plane bending vibration of the vinyl group in "trans" configuration.[20,21] Also, the out-of-plane modes giving strong bands around 700 cm^{-1} in TSB and DSB can easily be assigned to vibrations of the external rings, since they are not present in the PPV spectrum. As in Raman, a close inspection of these ir spectra enables to establish some filiations. Thus, among the DSB bands at 1014, 1026, and

TABLE I. Attributed and calculated frequencies ($0-1650$ cm^{-1} range) of Raman active in-plane vibrations of TSB, DSB, and PPV. In the table, e.c. stands for vibrations of external aromatic cycles, i.c. for vibrations of internal aromatic cycles, V. for vibrations of vinyl groups. n.o. are nonobserved but calculated frequencies and the question mark (?) indicates the observed bands that have not been used in the fit.

D_{6h}	Benzene obs	calc.	e.c.	v.	TSB obs	calc.	e.c.	i.c.	v.	DSB obs	calc.	i.c.	v.	PPV obs	calc.
V_g				*	1638	1626			*	1632	1632		*	1625	1636
$E_{2g,a}$	1596	1596	*		1592	1591	*	*		n.o.	1612	*			
										1588	1589			1582	1587
$E_{2g,b}$	1596	1596	*		1571	1571	*	*		1574	1576	*			
										1556	1546			1546	1538
$E_{1u,a}$	1479	1482	*		1491	1489	*			1491	1493				
$E_{1u,b}$	1479	1482	*		1445	1447	*			1447	1451				
V_u									*	n.o.	1342				
A_{2g}	1346	1345	*		1339	1338	*	*		1335	1335	*		1327	1329
V_g				*	1326	1315			*	1321	1316		*		
										1304	1289			1301	1295
B_{2u}	1309	1308			?1260	1268				1266	1266				
$E_{2g,b}$	1178	1179	*				*	*		n.o.	1243				
V_g				*	1192	1198			*	1193	1195		*	1197	1192
$E_{2g,a}$	1178	1179	*		1182	1174	*	*		1178	1175	*			
										n.o.	1167			1170	1163
B_{2u}	1149	1150	*		1154	1151	*			1157	1150				
$E_{1u,b}$	1036	1033	*		n.o.	1075	*			n.o.	1076				
$E_{1u,a}$	1036	1033	*		1026	1026	*			1028	1026				
B_{1u}	1010	1010	*		996	1006	*			997	1006				
A_{1g}	992	992	*				*			879	889	*		887	896
					866	864		*		858	850				
$E_{2g,a}$	606	606	*		640	637	*			650	647	*		662	660
										?618	614				
$E_{2g,b}$	606	606	*		n.o.	602	*	*		n.o.	603	*		?634	603
V_u	$T_\parallel$								*	519	516				
V_u	$T_\perp$								*	n.o.	494				
A_{2g}	Rot		*		?290	273	*	*		?299	283	*		327	311
$E_{1u,a}$	$T_\parallel$		*		n.o.	174	*			?132	128				
$E_{1u,b}$	$T_\perp$		*				*			?71	75				
						Rot					Rot				

1072 cm^{-1}, the first one corresponds to 1013 cm^{-1} in PPV (internal cycle), and the two others correspond to 1028 and 1072 cm^{-1} in TSB (external cycles). Some difficulties arise however in the interpretation of those spectra because of the excess of observed bands as compared with the predicted number of B_u modes. Even having separately carried out the attribution of out-of-plane vibrations, some extra bands may be due to combination transitions. Examples of the choices that had to be made in the assignments will be discussed later.

3. Oriented PPV

Raman or ir spectra recorded with nonpolarized light on highly oriented PPV films are rigorously identical to those described above. Thus, stretching the polymer does not modify the intrachain structure. Polarized Raman spectra, which are likely to give information about the polarizability tensor, do not show clear intensity differences when we use different configurations. In contrast, polarized ir (Fig. 5) present a strong dichroism which has been already reported.[46] Intensities of some absorption lines strongly depend on the orientation of the incident electric field. For instance, out-of-plane modes peaked at 555, 560, 837, and 966 cm^{-1} almost completely vanish when the light polarization is parallel to the stretching direction. Hence it can be inferred that polymer chains are almost parallel to this direction, in agreement with x-ray-diffraction observations on oriented PPV.[47] Further, the angle α between the polymer axis and the induced dipolar moment $\boldsymbol{\mu}$ can be estimated for each band. A cylindrical distribution for the orientations of molecular planes has been assumed, considering that the $\mu_\parallel = \mu \cos\alpha$ component is entirely excited, whereas for $\mu_\perp = \mu \sin\alpha$, only its projection on the polarization direction is effective. The absorbance $A_\parallel$ ($A_\perp$) is proportional to $\mu_\parallel^2$ (resp. $\mu_\perp^2$), so that the corrected relation is $tg^2\alpha = 2\,A_\perp/A_\parallel$. Resulting α values will be compared with the ones obtained from the modelization (Table III). Yet, from the residual parallel intensities of out-of-plane vibrations, which should in

TABLE II. Attributed and calculated frequencies ($0-1650$ cm^{-1} range) of infrared active in-plane vibrations of TSB, DSB, and PPV. In the table, e.c. stands for vibrations of external aromatic cycles, i.c. for vibrations of internal aromatic cycles, V. for vibrations of vinyl groups. n.o. are nonobserved but calculated frequencies and the question mark (?) indicates the observed bands that have not been used in the fit.

D_{6h}	Benzene obs	calc.	e.c.	v.	TSB obs	calc.	e.c.	i.c.	v.	DSB obs	calc.	i.c.	v.	PPV obs	calc.
V_g									*	n.o.	1622				
$E_{2g,a}$	1596	1596	*		1597	1608	*			1595	1596				
$E_{2g,b}$	1596	1596	*		1577	1579	*			1573	1575				
										1511	1509	*		1518	1516
$E_{1u,a}$	1479	1482	*		1495	1497	*	*		1486	1491				
$E_{1u,b}$	1479	1482	*		1451	1457	*	*		1446	1453	*			
										1417	1428			1424	1436
A_{2g}	1346	1345	*		1336	1343	*			1339	1342				
V_u				*	1331	1322			*	1332	1328		*	1340	1333
V_g									*	1306	1317				
V_u				*	1266	1266			*	1267	1268		*	1271	1269
B_{2u}	1309	1308	*		1219	1237	*	*		n.o.	1259	*			
$E_{2g,b}$	1178	1179								1213	1212				
V_g									*	1192	1183			1179	1181
$E_{2g,a}$	1178	1179	*		1183	1176	*			1180	1174				
B_{2u}	1149	1150	*		1154	1150	*			1154	1151				
									*	1114	1116	*		1107	1117
$E_{1u,b}$	1036	1033	*		1072	1076	*			1072	1076				
$E_{1u,a}$	1036	1033	*		1028	1027	*	*		1026	1027	*			
										1014	1025			1013	1026
B_{1u}	1010	1010	*		1002	1007	*	*		998	1006	*			
A_{1g}	992	992	*		n.o.	837	*			?846	856				
									*	797	809			784	787
$E_{2g,b}$	606	606	*		619	611	*			619	612				
$E_{2g,a}$	606	606	*		540	539				593	584				
V_u	$T_\perp$			*	468	468			*	451	449		*	428	425
										279	285				
A_{2g}	Rot		*		n.o.	70	*			n.o.	168				
$E_{1u,b}$	$T_\perp$		*				*	*		n.o.	32	*			
$E_{1u,a}$	$T_\parallel$		*		$T_\perp,T_\parallel$		*	*		$T_\perp,T_\parallel$		*		$T_\perp,T_\parallel$	

principle have a strictly perpendicular polarization, the non-oriented fraction in the sample has been estimated to be less than 3%.

C. Theoretical results

1. Valence force field

The set of force constants resulting from the optimization process and representing the valence force field (VFF) for PPV series is given in Table IV. Each force constant is defined in relation with the variation of internal coordinates R_i, R_j according to the expression

$$F_{R_i R_j} = \left(\frac{\partial^2 U}{\partial R_i \partial R_j} \right)_0,$$

where U is the vibrational potential energy. In Table IV, force constants are arbitrarily separated in four groups. In order to ensure the global coherence between all vibrational studies performed on aromatic polymers, the benzene model[13] has been used to characterize the part of phenylene
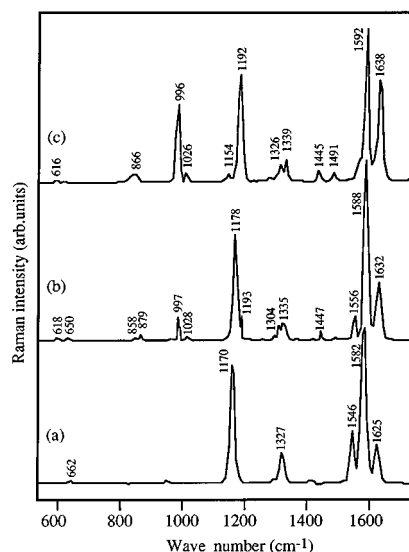
FIG. 3. Raman spectra recorded at 300 K with $\lambda_L = 1064$ nm of (a) PPV, (b) DSB, (c) TSB.
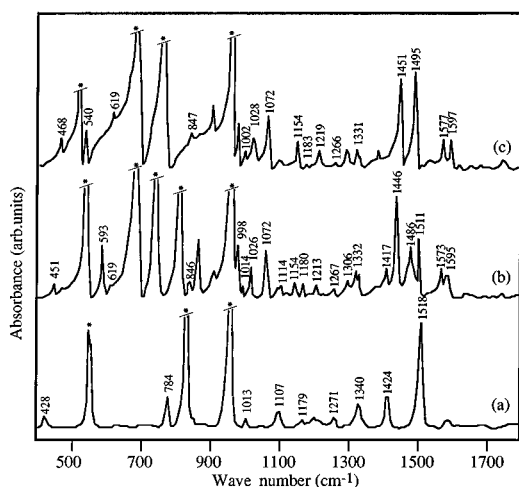
FIG. 4. Infrared spectra recorded at 300 K of (a) PPV, (b) DSB, (c) TSB.

rings that is not perturbed by the parasubstitution. The same set of parameters has already been used in the dynamical study of other series related to aromatic polymers.[37–39] Such a procedure has led to the determination of the semiempirical relationship (1) between carbon-carbon bond lengths and the corresponding stretching force constants.[15]

This relation traduces the link between vibrational frequencies and bond stiffness. In the fitting process for the PPV series, the carbon-carbon stretching force constants F_{R^2}, F_{D^2}, and $F_{t'^2}$ were allowed to vary from values predicted by relation (1), whereas F_{t^2} was kept constant to the value found in the benzene model. Figure 6 shows that the optimized values reflect the different bond orders: $F_{t'^2}$ is close to F_{t^2}, as expected for an aromatic ring, and they both correspond to an average between F_{R^2} and F_{D^2}. The force constant $F_{s'^2}$, related to the C-H stretching on the vinyl group, has been obtained by taking into account the assignment of the TSB high-frequency modes (at approximately
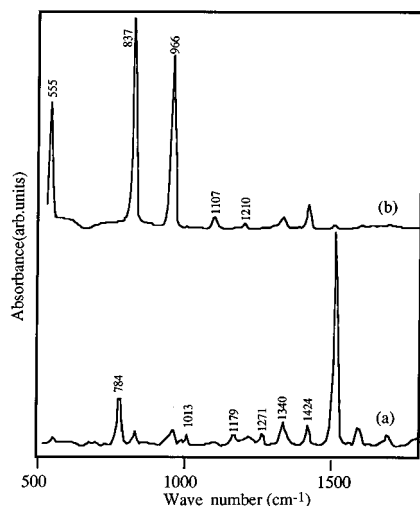
FIG. 5. Polarized infrared spectra (300 K) of highly oriented PPV films; polarization is parallel (a) or perpendicular (b) to the stretching direction.

TABLE III. Observed and calculated polarizations of infrared-active modes in PPV. Experimental angle values ($\pm 10°$) are relative to the stretching direction of a highly oriented sample, and calculated angle values are relative to the polymer axis.

Frequencies (cm^{-1})			Polarizations	
Expt.	Calc.	α	Expt.	α calc.
1518	1516	10	($\parallel$)	11°
1424	1436	60		43°
1340	1333	50		59°
1302[a]		50		
1271	1269	30		19°
1210[a]		c	($\perp$)	
1179	1181	10	($\parallel$)	12°
1107	1117	75		76°
1013	1026	30		10°
966[b]		85	($\perp$)	
837[b]		85	($\perp$)	
784	787	0	($\parallel$)	5°
555[b]		85	($\perp$)	
428	425	d		43°

[a]Experimental bands not attributed.
[b]Bands attributed to out-of-plane vibrations.
[c]A numerical value cannot be estimated, due to an overlap with a broad band.
[d]Out of the detection range of the microbeam apparatus used for these measurements. However, using another device, α exp. has been estimated to be less than 45°.

3000 cm^{-1}) performed by Meic and Güsten on deuterated TSB spectra.[41] Its final value is close to the corresponding force constant F_{s^2} in the benzene model (respectively, 4.90 and 5.09 mdyn/Å). Concerning the angular degrees of freedom around each sp^2 carbon atom, the internal coordinates defined in Fig. 7 are redundant since three angles are taken into account whereas two would be sufficient. Redundancy problems are brought out by considering only three independent force constants related to the relevant angular internal coordinates. Choice has been made of bending force constants of ''F_{α^2}''-type. Indeed, such a definition of each carbon atom environment enables to compare similar carbon neighborhoods in different molecules. For instance, values of bending force constants around the quaternary carbon remain close to the benzene ones ($F_{\alpha^2} \approx F_{\alpha'^2}$ and $F_{\phi^2} \approx F_{\phi''^2}$). For the C-C=C bending of the intercycle, one obtains $F_{\beta^2} \approx F_{\phi'^2}$, and smaller values for C=C-H and C-C-H bendings ($F_{\beta'^2} > F_{\beta''^2}$). It makes sense that these force constants are ordered according to the stiffnesses for bending oscillations. On the other hand, no clear interpretation is available for the force constants which involve two different internal coordinates. During the fitting process, it has been possible to reduce the number of those parameters in order to reinforce the physical meaning of the final model, keeping in mind that the loss in frequency adjustment is negligible. Thus, the VFF model for PPV series consists in 34 force constants and among them 11 have been fixed (from benzene) and 23 optimized.

2. Assignment of vibrational modes and calculation results

The assignment of Raman and ir experimental vibrational modes of TSB, DSB, and PPV is reported in Tables I and II.

TABLE IV. Valence force field for PPV series; optimized in-plane force constants.

Valence force constants in the unperturbated part of the aromatic ring;
benzene valence force field:

F_{t^2}	6.21^a	F_{α^2}	1.04^b	F_{1tt}	0.85	$F_{s\alpha}$	-0.13
F_{s^2}	5.09	F_{ϕ^2}	0.50	F_{2tt}	-0.31	$F_{t\alpha}$	0.11
				F_{3tt}	0.33	$F_{t\phi}$	0.16
						$F_{\phi\phi}$	0.02

Valence force constants in the part of the ring perturbated by the intercycle:

$F_{t'^2}$	6.18	$F_{\alpha'^2}$	1.07			$F_{t'\phi'}$	0.42
		$F_{\phi'^2}$	0.82			$F_{t'\alpha'}$	0.26
		$F_{\phi''^2}$	0.49				

Valence force constants coupling the aromatic ring and the vinyl group:

F_{R^2}	5.15			$F_{t'R}$	0.51	$F_{\alpha'R}$	-0.42
				$F_{t'D}$	-0.20	$F_{\beta\phi'}$	0.11
				$F_{1t'D}$	-0.30		

Valence force constants in the vinyl group:

F_{D^2}	7.23	F_{β^2}	0.80	F_{RD}	0.53	$F_{\beta'D}$	0.19
$F_{s'^2}$	4.90	$F_{\beta'^2}$	0.61	F_{RR}	-0.27	$F_{\beta R}$	0.30
		$F_{\beta''^2}$	0.50			$F_{\beta''R}$	0.28
						$F_{\beta'\beta'}$	0.09

[a] F_r2-type force constants, related to stretching vibrations, are expressed in mdyn $Å^{-1}$.

[b] $F_\theta2$-type force constants, related to bending vibrations, are expressed in mdyn $Å$ rad^{-2}.

These tables are organized in a way to put in evidence filiations from benzene ring and vinyl group vibrations. While experimental frequencies are known for benzene, the frequencies of the vinyl group vibrations have been indicated assuming some hypothesis. Generally, the characteristics of the vibrations of individual entities contribute to several modes whose frequencies are close to each other. It turns out that spectral ranges into which such ''mixtures'' occur can be distinguished as shown in Tables I and II. In these tables,
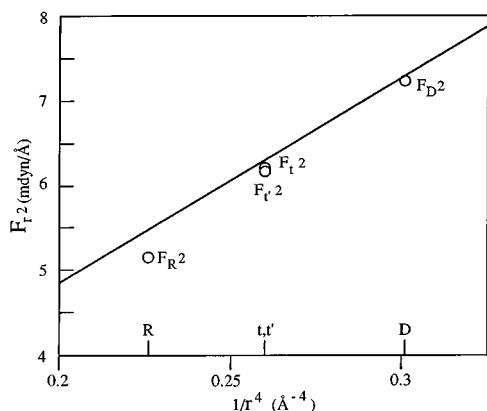
FIG. 6. Semiempirical relationship between carbon-carbon force constants F_r^2 and related carbon-carbon bond lengths r (from Ref. 15) and calculated in this work for PPV (circles).
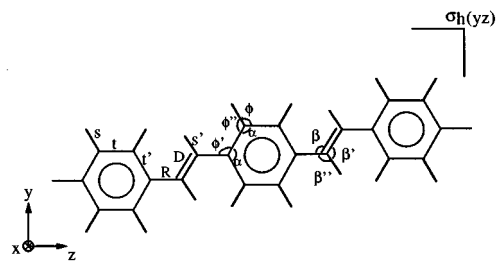
FIG. 7. Definition of the internal coordinates used in DSB. The geometric parameters used in our calculations are $t=t'=1.40$ Å, $s=s'=1.06$ Å, $R=1.45$ Å, $D=1.35$ Å, $\alpha=\alpha'=120°$, $\phi=\phi'=120°$, $\beta=126°$, $\beta'=114°$, $\beta''=120°$.

we have indicated by stars for each compound the number of in-plane modes below 2000 cm^{-1}. Calculated frequencies are also reported, as obtained from the VFF previously described. A good agreement with experimental values is obtained, with an average quadratic error of ~ 5 cm^{-1} for the least square fit. A few observed and weak bands whose assignment is too doubtful have not been fitted. On the whole, the VFF model being optimized on a set of 92 frequencies, their choice among the numerous observed bands is obviously decisive. Some particular points are discussed in the following, in light of useful additional information provided by our calculations: (i) The representation of atomic displacements indicates the original symmetry of each normal mode. It can also be qualitatively related to the observed intensities. (ii) For each normal mode, the potential energy distribution (PED) (Ref. 48) yields the contributions of the different force constants expressed in percents, providing a quantitative and complementary information to point (i). (iii) A simplified calculation of the induced dipolar moment for B_u modes in PPV yields a vectorial entity whose orientation can be compared to the polarized ir-absorption data.

3. Frequency range 1500–1650 cm^{-1}

In this range, three bands are observed in the PPV Raman spectrum at 1546, 1582, and 1625 cm^{-1}, respectively. At this point, it may be useful to compare with the Raman spectrum of poly(paraphenylene) (PPP) (Ref. 37). This aromatic polymer presents one very strong band at 1595 cm^{-1} accompanied by a very weak shoulder on the high-frequency side, attributed to A_g and B_{3g} vibrations of the disubstituted benzene (D_{2h} symmetry). The observation of an additional band in the same frequency range in PPV is obviously due to an A_g vibration of the vinyl group. By comparison with studies performed on compounds containing vinyl groups, it has been shown that a mode appears in this frequency domain, which is assigned to the symmetric stretching vibration of the C=C bond.[49,50] In the case of PPV, the coupling between the vibrations of the benzene ring and those of the vinyl group can be examined through the atomic displacements displayed in Fig. 8 and also through the PED's calculated for the modes mentioned above, the main ones being given in Table V. In contrast with the case of PPP, the B_{3g} character, mainly represented by $F_{t'2}$ contribution, is clearly associated with the lower frequency mode calculated at 1538 cm^{-1}. A detailed examination of this peculiarity shows
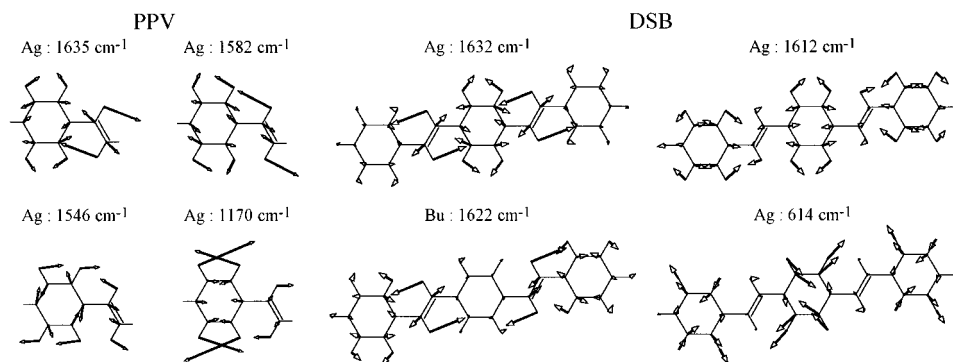
FIG. 8. Representation of atomic displacements of PPV in the left side; DSB in the right side.

that this frequency shift is attributable to the intercycle in PPV, the single C-C bond in PPP being replaced by the vinyl group. A quantitative signature has been found by a lower PED value for $F_{\phi'2}$ in PPV than in PPP (2% and 10%, respectively) that can explain the frequency lowering. On the other hand, the C=C stretching mode of the vinyl group principally couples with the A_g ring vibration, as can be observed in the two higher frequency modes. They present opposite phase relations between cycles and intercycles and the F_{D2} PED value is larger for the mode calculated at 1636 cm^{-1}, indicating that the vinylene C=C stretching provides its strongest contribution on this mode. This last point is to be retained for the discussion in Sec. IV. Another remark about this higher frequency mode can be added, when following its evolution along the PPV series. Its frequency decreases significantly when going from the shortest oligomer to the polymer: it is observed at 1638 cm^{-1} in TSB, 1632 cm^{-1} in DSB, 1629 cm^{-1} in distyryl-stylvene (not shown), and finally, 1625 cm^{-1} in PPV. Such a frequency lowering is significative of a modification of the electronic distribution on the intercycle. It is reasonable to argue that the conjugation extension on longer chains increases the electronic delocalization, with the effect of softening the C=C bond of the vinyl group. In contrast, a much higher frequency is reported for the C=C stretching mode in non-conjugated molecules containing a vinyl group: for example, it is observed at 1682 cm^{-1} in the trans-2-butene.[51] It can be noticed (Table I) that calculated frequencies increase from TSB to PPV by $\approx$ 10 cm^{-1}. This discrepancy with experimental values is due to the use of a same VVF model for both oligomers and PPV. A more refined calculation would require to decrease the value of F_{D2} when increasing the chain length.

TABLE V. PED's of the carbon-carbon stretching force constants for the three Raman-active modes in the 1600 cm^{-1} range in PPV.

Frequencies (cm^{-1})		PED (%)			
Expt.	Calc.	F_{t2}	$F_{t'2}$	F_{R2}	F_{D2}
1625	1636	23	17	0	23
1582	1587	21	25	16	17
1546	1538	0	65	6	10

4. Intensities

Qualitatively, one can consider that the intensity of Raman modes arises from the distortion of the π electronic cloud, together with specific phase relations between the local vibrations involving the different molecular groups. Thus, it is justified to calibrate Raman spectra intensities in PPV series on the band at $\sim$ 1580 cm^{-1}, owing to the nature of the corresponding normal modes. They take place on the whole molecule, with in-phase vibrations of all rings and all vinyl groups, the displacements being the same as shown in Fig. 8. The strong intensity of the mode observed at 1170 cm^{-1} in PPV, while it originates from a weak E_{2g} mode at 1178 cm^{-1} in benzene, can be attributed to the C-C bond stretching involving the R internal coordinate of the intercycle (Fig. 8). Indeed, such a vibration implies in-phase deformations of π electronic clouds on both cycles and intercycles along the conjugated chain. Since this property also holds for the strong band at $\sim$ 1580 cm^{-1}, it appears that the Raman intensity in PPV series is mainly connected with the R stretching. Consequently, these modes are characterized by a high PED for F_{R2}. The next point to be discussed concerns the intensities of a few DSB modes which are not observed (mentioned as ''n.o.'' in Tables I and II). In the case of A_g modes, the corresponding eigenvectors are characterized by out-of-phase vibrations of the different groups, as can be noticed in Fig. 8 for the modes calculated at 1612 and 614 cm^{-1}. This peculiarity can explain why they are not observed. A different case arises with the B_u mode predicted at 1622 cm^{-1}. It contains ''g''-type vibrations on both cycles and vinyl groups (Fig. 8). Such vibrations are inactive in ir absorption, even after the modifications caused by the substitution. Substituted carbons do not show significant displacements, suggesting a weak induced dipolar moment. On the contrary, the corresponding A_g mode at 1632 cm^{-1} is relatively strong in the DSB Raman spectrum.

5. Polarization of B_u modes in PPV

The validity of our model can also be checked through the comparison between experimental data obtained in polarized ir absorption on oriented PPV films, and the polarization of ir-active modes that can be deduced from the calculated atomic displacements. Induced variations of the dipolar moment principally arise from the relative displacements of carbon and hydrogen atoms. In a simplified representation, we have considered $\mu \propto \Delta \mathbf{r}_H - \Delta \mathbf{r}_C$. From the components of

this vectorial entity, the angle between μ and the polymer axis can easily be computed for each mode. Calculated and observed polarizations reported in Table III show a good agreement. Let us recall that the polarization angle deduced from the experiment is relative to the stretching direction. We already noticed in Sec. III B that this direction can be considered in a good approximation to be parallel to the polymer axis. Hence the comparison between calculated and experimental values is justified. Such an analysis is also helpful for the attribution of the two B_u modes expected in the 1180–1300 cm^{-1} range. Five bands are observed at 1179($\parallel$,w), 1194($\parallel$,vw), 1210($\perp$,w), 1271(30°,m) and 1302 cm^{-1} (50°,vw). The two expected B_u modes originate from a vinyl translation mode of u symmetry and from a B_{2u} mode of benzene, both antisymmetric in regard to the z axis defined in Fig. 7. Consequently, the resulting dipolar moment might be rather parallel to z or, say, to the polymer axis (the angle between them is ~10°). Calculated polarizations actually matched this property, even when no assignment was imposed for these frequencies. Taking into account these arguments together with those deduced from intensities and filiations from oligomers, we assigned the bands observed at 1179 and 1271 cm^{-1}.

6. Effects of symmetry breaking in PPV

Going back to symmetry considerations and their consequences on normal modes, an interpretation can be proposed for some extra bands regularly observed in PPV spectra. For instance the ir band peaked at ~1595 cm^{-1} is a reminiscence of an A_g mode observed in benzene at 1596 cm^{-1}. In finite length chains, this mode yields an ir-active antisymmetric combination. This is the case of the bands peaked at 1597 cm^{-1} in TSB and 1595 cm^{-1} in DSB. For the infinite PPV chain, the presence of an inversion center on all the cycles implies that this combination is inactive. Consequently, the observation of a weak band in the ir spectrum of the actual polymer puts in evidence the possibility of having cycles without an inversion center. This can be the case for cycles on chain ends. Another possibility would be the occurrence of a different conformation for the polymer chains. For instance with a ''boat'' configuration instead of the commonly assumed ''arm-chair'' one, the symmetry becomes D_{2h}. The unit cell is doubled and the inversion center on the phenylene ring is removed. Without studying this case extensively, such hypothesis could also explain the Raman band systematically observed at 1414 cm^{-1} in the PPV spectrum. A symmetric combination between vibrations of B_{2u} origin involving rings free of inversion center would then become active. However, if such symmetry defects are likely to be present in dilute concentration, one can consider our modelization in the ''arm-chair'' configuration the most appropriate to explain our results in the case of infinite chains.

7. Concluding remarks on neutral PPV

Establishing a VFF model for PPV has been supported by the joint study of a series of oligomers with the aim to improve the assignment of all vibrational modes. Even though some of them can still be questioned, the VFF model presented in this section provides a wide diversity of information. Thus, it can be considered as representative of the dy-
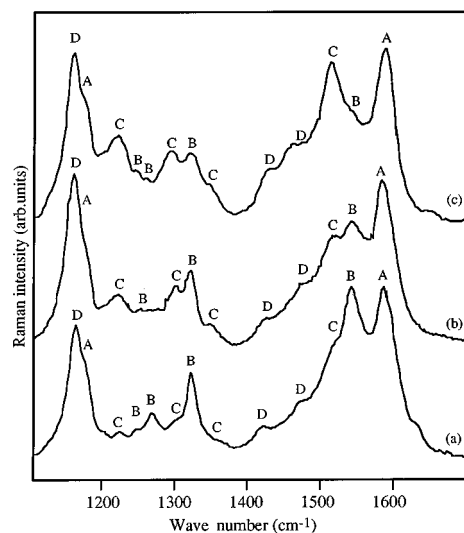

FIG. 9. Resonance Raman spectra of PPV-Na at maximum doping level, recorded with (a) $\lambda_L = 514.5$ nm; (b) $\lambda_L = 676.4$ nm; (c) $\lambda_L = 1064$ nm.

namical behavior of this series of compounds. In addition, this model also succeeds in determining the vibrational frequencies of another series of substituted oligomers.[52] In the following section, it will be extensively used to study the conducting state of PPV, including the relation (1) between carbon-carbon stretching force constants and corresponding bond lengths. Therefore, this approach can be used to study fruitfully the perturbations induced by doping along the polymeric chains.

IV. DYNAMICAL STUDY OF THE N-TYPE DOPED CONDUCTING STATE

A. Experimental results with sodium-doped PPV

1. Resonance Raman scattering

Two complementary ways of inspecting the spectral modifications occurring in the case of n-type doping have been carried out. First, the comparison of spectra recorded on a given sample with different excitation wavelengths (hereafter referred as λ_L) enables to stress out resonance effects. Second, choosing one given excitation, the spectral changes are followed as the doping rate is increased.

Let us first examine sodium-doped PPV films at the maximum doping level. Figure 9 shows the RRS spectra when changing the excitation wavelength from the green range ($\lambda_L = 514.5$ nm) to the near-infrared range ($\lambda_L = 1064$ nm). The main modifications arise in the 1100–1700 cm^{-1} range. New Raman bands are observed, whose relative intensities depend on the excitation line whereas their positions remain unchanged. A further analysis enables to distinguish several groups of bands which exhibit different resonance behaviors. Bands labeled A obviously originate from the two strongest bands of neutral PPV at 1170 and 1582 cm^{-1}, with the same maximum frequencies but being broadened. Their intensity remains roughly constant whatever the excitation wavelength. New bands appear at other frequencies, whose values are collected in Table VI. Bands labeled B are resonantly

TABLE VI. Raman frequencies (in cm^{-1}) observed in sodium-doped PPV. Labels correspond to those mentioned in Figs. 9 and 10.

($\lambda_L = 514.5$ nm)	($\lambda_L = 676.4$ nm)	($\lambda_L = 1064$ nm)	Label
1624			
1581	1578	1583	A
1536	1537	1539	B
1510	1509	1508	C
1465	1465	1455	D
1412	1414	1425	D
	1340	1344	C
1315	1312	1312	B
1293	1290	1287	C
1260		1250	B
1240	1245	1240	B
1217	1215	1216	C
1171	1172	1174	A
1158	1155	1156	D

enhanced with $\lambda_L = 514.5$ nm (2.41 eV), whereas their relative intensity decreases when the excitation goes to the red range (676.4 nm, 1.83 eV) and further to the near ir range (1064 nm, 1.16 eV). In contrast, the resonance of bands labeled C occurs with the near ir excitation. For the last group of new bands labeled D, no significant resonance effect is observable. This RRS study demonstrates that the n-type doping induces the coexistence of several species, which can be related to different kinds of defects along the polymer chains. In this case, different electronic transitions can contribute to the overall RRS and their contribution may have different sign causing interference effects. However, Raman bands are resonantly enhanced when the excitation is close to a specific transition of a given species. Consequently, it is appropriate to attribute ''B'' bands to one species whose absorption is presumably close to 2.4 eV, and ''C'' bands to another whose absorption can presumably be in the range of 1 eV. The additional ''D'' bands and the broadened ''A'' bands can originate either from vibrational modes common to the above mentioned species, or from species having an absorption band spread over a wide energy range. Also, the presence of unperturbated segments is still observed when using excitations within or close to the absorption band of neutral PPV (at ~3 eV). Thus, even at the highest doping levels, the isolated band at 1625 cm^{-1} characteristic of the vinyl C=C stretching mode in neutral PPV is still observed when using $\lambda_L = 514.5$ nm. Moreover, spectra recorded with shorter wavelengths (i.e., higher excitation energies) present a strong fluorescence from which the only bands of neutral PPV emerge.

Other alkaline counter-ions can be used to obtain n-type doped PPV. It is noticeable that spectra Figs. 9(b) and 9(c) are very similar to those reported for potassium-doped PPV with 752 and 1064 nm excitation lines.[53] This is consistent with the fact that Raman spectroscopy probes the doping-induced perturbations on the intrachain scale, independently from the counter ion responsible of the charge transfer.

The resonance behavior of the different groups of Raman bands described above provides qualitative information

about the energy ranges of electronic transitions of doping-induced species, which can be related to those issued from band-structure calculations. In a simple Hückel approximation (one-electron picture), polarons and bipolarons are associated to new energy levels localized within the energy gap of the polymer.[54,55] Two main subgap transitions are expected for polarons, whereas one main transition at a smaller energy is expected for bipolarons.[56] From a molecular spectroscopy point of view, corresponding transitions exist between the energy levels of radical anions or dianions of model compounds.[57,58] In conducting PPV and PPP, either in oxidized or reduced forms, two broad absorption bands within the energy gap are generally reported.[59–62] Thus, it is likely that the bipolaronic transition overlaps with the lowest energy one from the two polaronic transitions. Also in electron energy-loss spectroscopy spectra recorded with lightly doped PPV-Na samples, two broad peaks centered at 2.0 and 1.1 eV have been reported.[63] From these considerations, the RRS effects observed in Fig. 9 using three different excitation wavelengths are consistent with an attribution of ''B'' bands to polarons, and ''C'' bands to bipolarons. In this case, RRS is particularly appropriate to get qualitative information about the absorption features since direct optical spectra are difficult to obtain in highly doped polymers.

A suitable comparison can be made between our observations and the RRS study presented by Sakamoto and co-workers.[11] These authors also recorded Raman spectra of ''heavily doped'' PPV-Na samples at different excitation wavelengths, before and after annealing. However, some differences with our results seem to indicate that the doping level of their sample is lower than in ours. Spectra obtained with $\lambda_L = 1064$ nm are very similar to the one shown in Fig. 9(c), but with shorter excitation wavelengths, they exhibit different features which indicate a significant amount of neutral segments. On the other hand, these authors make a comparison with spectra of soluble model compounds containing one, two, or three vinyl groups (labeled $PV1$, $PV2$, and $PV3$) and reduced into radical anions or dianions. Indeed, strong analogies are evidenced between some Raman spectra of such short species and doped PPV. The greatest similarity is observed between PPV-Na and $PV3^{2-}$ spectra recorded with $\lambda_L = 1064$ nm [same as Fig. 9(c)]. Resonance effects are also demonstrated: excitation lines in the red or in the near ir range favors the observation of species like $PV3^{\cdot-}$ and $PV3^{2-}$, whereas shorter species like $PV1^{\cdot-}$, $PV1^{2-}$, $PV2^{\cdot-}$, and $PV2^{2-}$ are better observed with higher excitation energies. These effects are in agreement with the energies of the main electronic transitions of the reduced model compounds. Similar observations were reported by Furukawa and co-workers[58] from a RRS study carried out on PPP doped with sodium, and related model compounds of short lengths. Both approaches led to conclude to the coexistence of polarons and bipolarons of various lengths and short spatial expansion in doped polymers. Also, Sakamoto and co-workers[11] outlined the possible role of the morphology or solid-state structure of the real material in the presence of such localized excitations. Accordingly, it is likely that the PPV-Na samples we have studied do not contain exactly the same entities. Our results bring a complementary view on the complexity of the system and one can conclude to the coexistence of several doping-induced intrachain de-
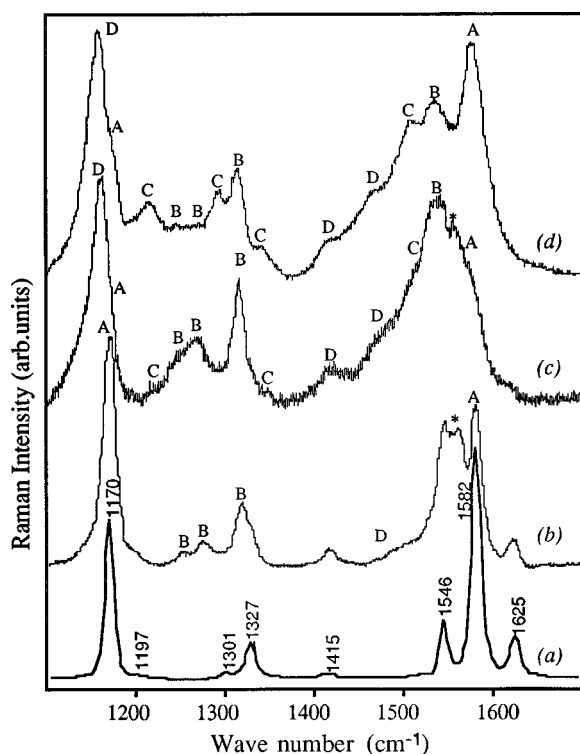
FIG. 10. Raman spectra of PPV-Na with a gradual doping level, $\lambda_L = 676.4$ nm. (a) Neutral PPV; (b) weak doping; (c) intermediate doping; (d) maximum doping level. (*)1560 cm^{-1}, not listed in Table VI, related to species appearing at low sodium concentrations.
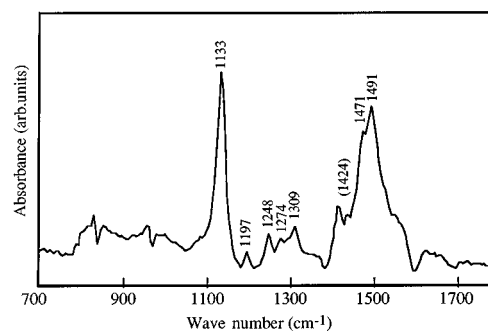

FIG. 11. Infrared spectrum difference during dedoping of PPV-Na.

induced bands recorded on Fig. 9, Fig. 10(b) exhibits a band at 1560 cm^{-1}. It appears at low doping levels and is analogous to the one reported by Sakamoto and co-workers[11] at 1564 cm^{-1} with $\lambda_L = 632.8$ nm. This feature is no longer seen at higher doping levels, due to the strong intensity of the bands at 1536 and 1580 cm^{-1}.

Additional reliable observations are issued from electron paramagnetic resonance studies on conducting polymers.[64–66] In these investigations, mobile spins related to the extrinsic doping-generated charge carriers are observed. During the gradual dopant insertion, the spin concentration first reaches a maximum at intermediate doping levels and then decreases. A thermodynamic interpretation has been proposed[67] in terms of an equilibrium displacement between polarons ($S = \frac{1}{2}$) and bipolarons ($S = 0$) depending on the charge transfer. Indeed, intensity variations observed in our RRS studies are consistent with such a picture. This argument confirms our attribution of bands from groups ''B'' and ''C'' to polarons and bipolarons, respectively.

2. Infrared spectra during dedoping

Infrared spectra of sodium-doped PPV were recorded during dedoping according to the following way. Films about 5 μm thick have been installed in a special cell allowing a gradual introduction of air. Therefore, a compensation process can take place with a slow kinetic. Once the ir transmission can be measured, spectra display doping-induced bands superimposed to those of pristine PPV. These new bands progressively vanish, which would not be the case if they were due to irreversible modifications such as chemical defects. Hence the difference spectrum presented in Fig. 11 is the ir signature of the polaronic and/or bipolaronic species. Some attempts to assign these features will be proposed in the next section.

B. Interpretation and discussion

1. Preliminaries

As a consequence of the charge transfer on polaronic and bipolaronic segments, theoretical studies have predicted changes in bond orders with a quinoid character [Fig. 1(d)].[8,9] From our experimental study, the disappearance of the stretching mode of the vinyl group at 1625 cm^{-1} puts in evidence a modification in the electronic distribution on the intercycle. The purpose of this section is therefore to account

fects. They are characterized by different absorption energies and confined on relatively short chain segments, and can be assimilated to polarons and bipolarons.

The second step in our experimental investigation had the purpose of following the spectral modifications as a function of the sodium content, using a given excitation line. When using $\lambda_L = 514.5$ nm, except for the highest doping level, only modes from neutral PPV are observable from a strong fluorescence background. Figure 10 displays Raman spectra recorded at $\lambda_L = 676.4$ nm with gradual doping levels. Results obtained with near ir excitation ($\lambda_L = 1064$ nm), which favors the observation of C bands, have been published in Ref. 14. The gradual transformation of neutral polymeric sequences into perturbated segments is evidenced by the vanishing of the Raman band at 1625 cm^{-1}. Its complete disappearance at the highest sodium ratios is due to the use of a red range excitation, since resonance conditions are not fulfilled for the remaining unperturbated chains. Following the sodium insertion from Figs. 10(b)–10(d), ''B'' bands increase until the intermediate sodium ratios and then decrease, while ''C'' and ''D'' bands keep on growing as a function of the doping level. These different behaviors confirm that those groups of bands are characteristic of several species coexisting in the material, with relative concentrations which depend on the charge transfer brought by the gradual dopant insertion. Using $\lambda_L = 1064$ nm confirms these changes in concentrations. Relative intensities are modified according to the different resonance conditions. For instance ''C'' bands that are favored by near ir excitation appear from the beginning of the doping. Notice that in addition to the doping-

for doping-induced vibrational modes by means of a modelization of charged segments, achieved via a perturbation of the VFF of the neutral compound. We first present the assumptions made in our calculations in order to limit the number of parameters allowed to vary.

Among force constants defined in Sec. III, those related to carbon-carbon stretchings are obviously the most sensitive against changes in bond orders. It is worth pointing out that the perturbation of the pristine structure is expected to be rather weak, in view of the frequency shifts which never exceed 3%. For this reason and also because of the limited number of experimental data, variations in the VFF were restricted to the four carbon-carbon force constants F_{R^2}, F_{D^2}, F_{t^2}, and $F_{t'^2}$. Other possible variations were thus neglected, principally those involving bending degrees of freedom. We have checked separately that they essentially participate on lower frequency modes and therefore have very little influence on the vibrational modes in the range $1000-1600$ cm^{-1}.

Another step consists in defining a geometric scheme for polaronic and bipolaronic segments. It is clear that the translation symmetry of the pristine polymer is lost, so we have used short length model-compounds. Chain segments equivalent to $PV2$ and $PV3$ oligomers are considered and the same geometric parameters as in the neutral form are used. Such a representation can be justified as follows:

(i) The length of these model compounds has been considered in view of some experimental observations.[11] Also, previous data have shown that the length is not a determining factor in vibrational calculations. Let recall that when studying the neutral series, a weak frequency dispersion has been obtained when the chain length is changed for experimental and calculated data. In spectra of charged model compounds (reduced[11] or oxidized[62]), frequencies can also be followed from one compound to the other since relatively small shifts are recorded. The small dependence of the vibrational frequencies versus the chain length can be taken into account. By contrast, strong intensity variations are observed with charged species. This behavior can be due to the charge confinement but electron-phonon interaction calculations would be needed to clarify this point.

(ii) Considering structures like $PV2$ and $PV3$ implicitly supposes that the C_{2h} symmetry is maintained in the charged segments. This assumption is also made in theoretical calculations and is reasonable for a weak range of perturbation of the original structure. Also, these two model compounds are of prior importance to examine the effects of an inversion center positioned either on a central intercycle ($PV2$) or on a central ring ($PV3$) on normal vibration modes.

(iii) The use of geometric parameters identical to those of neutral compounds is chosen in order to avoid redundancy. Any structural modifications that could appear on localized polaronic defects are deduced from variations in the force constants. However, we have also checked the influence of modified geometric parameters. Frequencies have been computed keeping the neutral VFF and using polaronic and bipolaronic geometries as predicted by theoretical calculations. We found no significant effect on calculated frequencies in the range $1100-1700$ cm^{-1}.

TABLE VII. Attribution of bipolaronic bands in sodium-doped PPV and calculation results for $PV3^{2-}$ model. Frequencies are in cm^{-1} and main PED contributions are indicated.

	Neutral PPV obs	Bipolaronic bands obs	calc.	Main contributions in PED
A_g	1625	n.o.	1635,1631[a]	$F_{t^2},F_{t'^2}$
	1582	1583	1578	F_{D^2},F_{R^2}
	1546	1508	1509	$F_{t'^2}$
	1327	n.o.	1310[a]	F_{D^2}
	1301	1287	1287	F_{D^2},F_{R^2}
	1197	1216	1213	F_{R^2}
	1170	1174	1176	F_{t^2}
		1156	1156,1148[a]	$F_{t'^2}$
B_u	1518	1491	1511	$F_{R^2},F_{t'^2}$
	1107	1133	1133	F_{t^2}

[a]Calculated in the same range, not fitted.

2. Modified valence force field

Variations in the four carbon-carbon force constants are obviously managed by the assignment of experimental bands. Polaronic and bipolaronic features have been considered separately and assignments were ensured by an iterative process. Doping-induced bands were examined successively on "PPV-like" infinite chains, $PV2$ and $PV3$ model-compounds. "A" bands have been taken into account in both polaronic and bipolaronic cases, since they appear in all spectra of our RRS study. These bands remain at the same frequencies as in the neutral polymer (1170 and 1580 cm^{-1}) and therefore traduce the stability of aromatic rings against modifications in the electronic distribution. As a consequence, parametrized force constants are maintained within relatively small variations. The weak D bands at approximately 1420 and 1460 cm^{-1} were not used in our fit, since they are not clearly assigned.

From the different sets of calculations, we found the fitting process much more reliable in the case of bipolaronic bands (A and C groups). This is why we present in this paper results for bipolaronic species only, whereas refinements for polaronic species are still in progress. Table VII collects the final assignments of $PV3^{2-}$ together with their calculated frequencies as compared to modes found in neutral PPV. The variations in carbon-carbon force constants are given in Table VIII. The strong Raman D band at 1156 cm^{-1} and the two strong ir bands at 1133 and 1491 cm^{-1} were only attributed in last fitting steps, taking into account that former calculations predicted the occurrence of modes in the same frequency range. If we take these bands into consideration, this leads to small deviations in our results. This "bipolaronic" species will be labeled $PV3^{2-}$ in the following.

TABLE VIII. Bipolaronic carbon-carbon force constants (mdyn Å^{-1}) in $PV3^{2-}$ model.

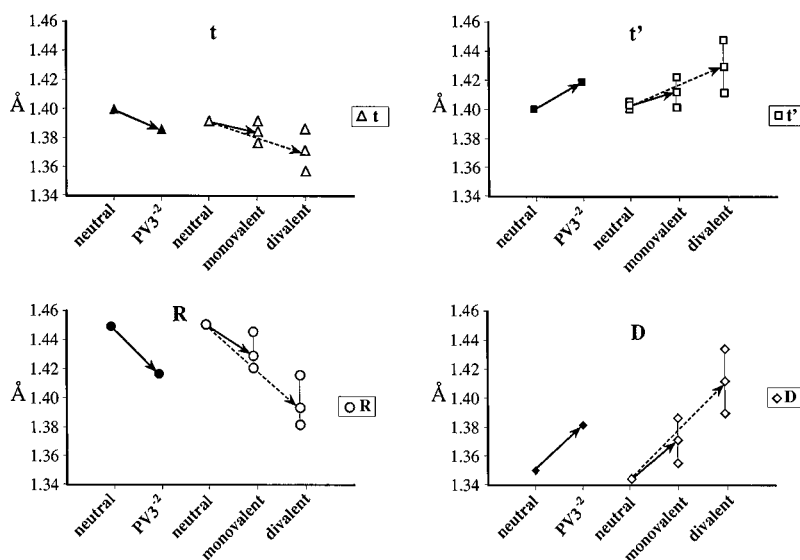|	F_{t^2}	$F_{t'^2}$	F_{R^2}	F_{D^2}
Neutral VFF	6.21	6.18	5.15	7.23
PV_3^{2-}	6.45	5.85	5.62	6.55

FIG. 12. Structural relaxation on bipolaronic segments. Comparison between variations in carbon-carbon bond length obtained from our calculations (filled symbols) and from geometric optimization methods (open symbols). In the latter case, the vertical segments represent the difference in parameters between central and external parts of $PV3$ model compounds.

Variations in force constants are clearly in agreement with the appearance of a quinoid character along the polymeric chain. Changes on the intercycle consist of an increase of F_{R2} and a decrease of F_{D2}, whereas the aromaticity in the cycles is modified with an F_{t2} force constant stronger than $F_{t'2}$. Relative variations in the two latter force constants are weaker than for F_{R2} and F_{D2}. Such a result seems to us acceptable according to simple arguments about bond orders around the quaternary carbon atom.

The main contributions among modified PED's are also given in Table VII. Let us examine the case of the vinyl stretching mode observed at $1625\,\mathrm{cm}^{-1}$ in neutral PPV, which vanishes after doping. In $PV3^{2-}$, two Raman modes are still calculated in the same range. However, F_{D2} which had a strong contribution in this vibration in neutral PPV is now involved in a mode of lower frequency calculated at $1578\,\mathrm{cm}^{-1}$. Therefore, one may deduce that the vanishing of this mode reflects the weakening of the double bond character on the vinyl group of PPV.

The next strong band assigned to bipolaronic species and observed at $1508\,\mathrm{cm}^{-1}$ originates from the neutral PPV mode at $1546\,\mathrm{cm}^{-1}$. From the values of modified PED, its frequency lowering may be attributed to the decrease in F_{D2} and $F_{t'2}$. On the other hand, F_{R2} contributions are moved towards higher frequencies, and the increase in this force constant explains the frequency shift from 1197 to $1216\,\mathrm{cm}^{-1}$. Variations in F_{t2} and $F_{t'2}$ are more difficult to follow, because their mutual influence are compensated in ring vibrations. As a consequence, the shape of the mode calculated at $1176\,\mathrm{cm}^{-1}$ is very much similar to the one observed at $1170\,\mathrm{cm}^{-1}$ in neutral PPV (Fig. 8). Concerning the strong band recorded at $1156\,\mathrm{cm}^{-1}$ in PPV-Na spectra, two modes are systematically calculated in this range. Also, we have not attempted to attribute all doping-induced ir bands. Nevertheless, among B_u vibrations, $PV3^{2-}$ model predicts modes which frequencies are close to the experimental ones peaked at 1491 and $1133\,\mathrm{cm}^{-1}$ and some of these values

have been used in last fitting steps. These bands may be interpreted as originating from the neutral PPV ir modes observed at 1518 and $1107\,\mathrm{cm}^{-1}$, respectively.

3. Structural modifications on bipolaronic defects

Using relation (1) between carbon-carbon force constants and corresponding bond lengths, the structural relaxation occurring on bipolaronic segments can be estimated. One obtains opposite variations of $\sim\pm2\%$ for D and R, and $\sim\pm1\%$ for t' and t. Variations in C-C distances are reported in Fig. 12 and are compared with those predicted by geometric optimization methods, taking into account that values describing the neutral state are consistent. Bond lengths in monovalent or divalent species are very similar from MNDO (Ref. 9) and $AM1$ (Refs. 8 and 36) calculations. These optimized geometries are generally determined by removing one or two electrons to lead to positively charged chains segments. Also, under the reasonable assumption of electron-hole symmetry in conducting polymers, the same parameters are considered for negative species. In addition, bond lengths obtained by these methods are slightly different in central and external parts of charged model compounds. This dispersion is shown in Fig. 12 together with averaged values. Notice that our vibrational model is uniform over all the compound and therefore, the bond lengths deduced from our calculations must be compared to the averaged values.

Keeping this point in mind, it is noticeable that C-C distances resulting from our vibrational analysis of bipolaronic bands are closer to the averaged optimized values calculated for monovalent species than to those calculated for divalent ones. Therefore, this represents a disagreement regarding the connection between structural relaxation and the nature of the charged species. We have confirmed this point by performing ''a contrario'' calculations. F_{R2}, F_{D2}, F_{t2}, and $F_{t'2}$ were modified according to the bond length predicted for the divalent compounds. The calculated frequencies are markedly different from the experimental ones attributed to bipo-

laronic species. We also have checked that the better agreement with monovalent values does not depend on the length of the model compound. Consequently, the discrepancy between vibrational and theoretical approaches could be an evidence that species identified as bipolarons induce weaker structural modifications than expected for entities with two excess electrons. It is worth noting that recent theoretical developments on conducting polymers propose that polarons and bipolarons could have a transverse character.[68] Localized excitations are no longer seen as being confined on one polymeric chain, but are transversely distributed over adjacent chains and inserted dopant counter-ions. This picture could explain that perturbations on PPV chains are weaker than expected when adding (or removing) two electrons. Other experimental results are consistent with such a transverse distribution. For instance, in some cases, NMR spectra of the dopant have indicated a significant probability for the conduction electrons to be located on sodium nucleus in PPV-Na,[69] or on cesium in CH_x-Cs.[70] On another hand, the assumption of electron-hole symmetry in conducting polymers has already been questioned.[71] It would imply the same relaxation for p-doped or n-doped systems. However, we have observed Raman spectra in p-doped PPV markedly different from those presented here.[72] Therefore, the modelization in the case of negative polarons or bipolarons compared to positive species will lead to different results. Refinements in the case of positive species are under way.

On the other hand, our modelization enables to compare variations in the different C-C bond lengths, instead of a global effective conjugation coordinate model.[73] We have adopted here a more classical picture that leads only to the determination of the vibrational mode frequencies but is not able to evaluate the relative intensity of these modes.

V. CONCLUSION

The vibrational study presented in this paper is devoted to the transformation from neutral to conducting PPV, observed at the intrachain scale. First, a valence force field has been established in order to investigate the dynamical properties of the neutral polymer and its associated series of oligomers. Among force constants, those related to carbon-carbon

stretchings are consistent with the relationship (1) previously established on numerous aromatic conjugated compounds, which enables to interpret bond length variations in polymeric systems.

The experimental RRS investigation of the conducting state, illustrated by sodium-doped PPV, has shown different groups of new bands. They have been attributed to short-length polarons and bipolarons coexisting in a thermodynamical equilibrium. Experimental data indicating an equilibrium between polarons and bipolarons and their relative stabilities are worth studying. First theoretical models based on ideal, isolated polymer chains predict bipolarons to be the stable charge carriers.[74,75] Since such a description, refinements have been made taking into account the effects of disorder and $3d$ or transverse interactions, either between adjacent chains or through the dopant.[68,76,77] The consequence is a new balance in their relative stability in favor of polarons, in better agreement with the several experimental observations of their existence even at high doping levels.

Doping-induced bipolaronic bands have been interpreted via a perturbation of the neutral valence force field performed on short-length model compounds. Variations in the electronic distribution are in agreement with a quinoid character along the polymeric chain. The changes in C-C bond lengths have been estimated, showing some discrepancies with theoretical predictions that could be connected to the transverse character mentioned above. Thus, the main interest of this vibrational study is to put in evidence the relaxation of the polymeric structure when charged species such as polarons or bipolarons are accommodated on PPV chains in terms of modifications in the valence force field.

[1] H. Shirakawa, E. J. Louis, A. G. MacDiarmid, C. K. Chiang, and A. J. Heeger, J. Chem. Soc. Chem. Commun. **1977**, 578.

[2] C. K. Chiang, M. A. Druy, S. C. Gau, A. J. Heeger, E. J. Louis, A. G. MacDiarmid, Y. W. Park, and H. Shirakawa, J. Am. Chem. Soc. **100**, 1013 (1978).

[3] C. K. Chiang, C. R. Fincher, Y. W. Park, A. J. Heeger, H. Shirakawa, E. J. Louis, S. C. Gau, and A. G. MacDiarmid, Phys. Rev. Lett. **39**, 1098 (1977).

[4] J. H. Burroughes, D. D. C. Bradley, A. R. Brown, R. N. Marks, K. McKay, R. H. Friend, P. L. Burn, and A. B. Holmes, Nature (London) **347**, 539 (1990).

[5] See, for example, H. Nakanishi, Nonlinear Opt. **1**, 223 (1991).

[6] G. R. Mölhmann, Synth. Met. **67**, 77 (1994).

[7] D. R. Baigent, N. C. Greenham, J. Grüner, R. N. Marks, R. H. Friend, R. C. Moratti, and A. B. Holmes, Synth. Met. **67**, 3 (1994).

[8] J. L. Brédas, D. Beljonne, Z. Shuai, and J. M. Toussaint, Synth. Met. **43/3**, 3743 (1991).

[9] H. Eckhardt, K. Y. Jen, L. W. Shacklette, and S. Lefrant, in *Conjugated Polymeric Materials: Opportunities in Electronics, Optoelectronics, and Molecular Electronics*, Vol. 182 of *NATO Advanced Study Institute, Series B: Physics*, edited by J. L. Brédas and R. R. Chance (Kluwer, Dordrecht, 1990).

[10] P. Brendel, A. Grupp, M. Mehring, R. Schenk, K. Müllen, and W. Huber, Synth. Met. **45**, 49 (1991).

[11] A. Sakamoto, Y. Furukawa, and M. Tasumi, J. Phys. Chem. **96**, 3870 (1992).

[12] S. Lefrant, E. Perrin, J. P. Buisson, H. Eckhardt, and C. C. Han, Synth. Met. **29**, E91 (1989).

[13] J. P. Buisson, J. Y. Mevellec, S. Zeraoui, and S. Lefrant, Synth. Met. **41-43**, 287 (1987).

[14] I. Orion, J. P. Buisson, J. Bullot, M. Spiesser, and S. Lefrant, C. R. Acad. Sci. Paris Ser. II b **320**, 515 (1995).

[15] S. Lefrant and J. P. Buisson, in *Frontiers of Polymer and Advanced Materials*, edited by P. N. Prasad (Plenum, New York, 1994), p. 289.

[16] R. A. Wessling and R. G. Zimmerman, U.S. Patent No. **3**, 401, 152 (Sept. 10, 1968).

[17] P. L. Burn, D. D. C. Bradley, A. R. Brown, R. H. Friend, and A. B. Holmes, Synth. Met. **41-43**, 261 (1991).

[18] D. A. Halliday, P. L. Burn, R. H. Friend, D. D. C. Bradley, and A. B. Holmes, Synth. Met. **55**, 902 (1993).

[19] J. Martens, N. F. Colaneri, P. L. Burn, D. D. C. Bradley, E. A. Marseglia, and R. H. Friend, *Lower Dimensional Systems and Molecular Electronics* (Plenum, New York, 1991), p. 393.

[20] I. Murase, T. Ohnishi, T. Noguchi, and T. Hiroka, Polymer **25**, 327 (1984).

[21] D. R. Gagnon, J. D. Capistran, F. E. Karasz, and R. W. Lenz, Polym. Bull. (Berlin) **12**, 293 (1985).

[22] R. W. Lenz, C. C. Han, J. D. Stenger-Smith, and F. E. Karasz, J. Polym. Sci., Part A: Polym. Chem. **26**, 3241 (1988).

[23] J. H. F. Martens, D. A. Halliday, E. A. Marseglia, D. D. C. Bradley, R. H. Friend, P. L. Burn, and A. B. Holmes, Synth. Met. **55**, 434 (1993).

[24] J. Stenger-Smith, R. W. Lenz, and G. Wegner, Makromol. Chem. **190**, 3005 (1989).

[25] J. Ghanbaja, J. F. Marêche, E. McRae, and D. Billaud, Solid State Commun. **60**, 87 (1986).

[26] D. Moses, N. Colaneri, and A. J. Heeger, Solid State Commun. **58**, 535 (1986).

[27] B. François and C. Mathis, Synth. Met. **16**, 105 (1986).

[28] D. Chen and M. J. Winokur, Phys. Rev. B **41**, 6759 (1990).

[29] R. Nuffer (private communication).

[30] C. J. Finder, M. G. Newton, and N. L. Allinger, Acta Crystallogr., Sect. B: Struct. Crystallogr. Cryst. Chem. **30**, 411 (1974).

[31] J. Bernstein, Acta Crystallogr., Sect. B: Struct. Crystallogr. Cryst. Chem. **31**, 1268 (1975).

[32] O. Lhost and J. L. Brédas, J. Chem. Phys. **96**, 5279 (1992).

[33] J. Obrzut and F. E. Karasz, J. Chem. Phys. **87**, 6178 (1987).

[34] D. E. King, J. E. Fernandez, and W. E. Swartz, Appl. Surf. Sci. **45**, 325 (1990).

[35] K. Gustav and A. Geyer, J. Prakt. Chem. **334**, 505 (1992).

[36] J. Cornil (private communication).

[37] J. P. Buisson, S. Krichene, and S. Lefrant, Synth. Met. **21**, 229 (1987).

[38] S. Zeraoui, Ph.D. Thesis, Université de Nantes, 1992 (unpublished).

[39] S. Quillard, G. Louarn, S. Lefrant, and A. G. MacDiarmid, Phys. Rev. B **49**, 12 496 (1994).

[40] H. S. Woo, O. Lhost, S. C. Graham, D. D. C. Bradley, R. H. Friend, C. Quattrocchi, J. L. Brédas, R. Schenk, and K. Müllen, Synth. Met. **59**, 13 (1993).

[41] Z. Meic and H. Güsten, Spectrochim. Acta A **34**, 101 (1978).

[42] G. Drefalhl, R. Kühmstedt, H. Oswald, and H. H. Hörhold, Makromol. Chem. **131**, 89 (1970).

[43] R. Mahrt, J. P. Yang, A. Greiner, H. Bässler, and D. D. C. Bradley, Makromol. Chem. Rapid Comm. **11**, 415 (1990).

[44] See, for example, S. Lefrant, J. Phys. (Paris), Colloq. **44**, C3-427 (1987); H. Kuzmany, Phys. Status Solidi B **97**, 521 (1980).

[45] J. Wery, B. Dulieu, E. Launay, J. Bullot, M. Baitoul, and J. P. Buisson, Synth. Met. **84**, 277 (1997).

[46] D. D. C. Bradley, R. H. Friend, H. Lindenberger, and S. Roth, Polymer **27**, 1709 (1986).

[47] T. Granier, E. L. Thomas, and F. E. Karasz, J. Polymer Sci. Polym. Phys. Ed. **24**, 2793 (1986).

[48] A. Alix, Spectrosc. Lett. **14**, 441 (1981).

[49] J. Y. Mevellec, J. P. Buisson, S. Lefrant, H. Eckhardt, and K. Y. Jen, Synth. Met. **35**, 209 (1990).

[50] G. Louarn *et al.*, in *Electronic Properties of Polymers*, edited by H. Kuzmany, M. Mehring, and S. Roth, Springer Series in Solid State Science Vol. 107 (Springer, Berlin, 1992), p. 298.

[51] A. Sakamoto, Y. Furukawa, and M. Tasumi, J. Phys. Chem. **96**, 1490 (1992).

[52] Y. Furukawa (private communication).

[53] A. Sakamoto, Y. Furukawa, and M. Tasumi, Synth. Met. **55/1**, 593 (1993).

[54] J. L. Brédas, R. R. Chance, and R. Silbey, Phys. Rev. B **26**, 5843 (1982).

[55] A. J. Heeger, S. Kivelson, J. R. Schrieffer, and W. P. Su, Rev. Mod. Phys. **60**, 781 (1988).

[56] K. Fesser, A. R. Bishop, and D. K. Campbell, Phys. Rev. B **27**, 4804 (1983).

[57] J. M. Oberski, A. Greiner, and H. Bässler, Chem. Phys. Lett. **184**, 391 (1991).

[58] Y. Furukawa, H. Ohtsuka, and M. Tasumi, Synth. Met. **55**, 516 (1993).

[59] G. Froyer, Y. Pelous, F. Maurice, M. A. Petit, A. Digua, and J. F. Fauvarque, Synth. Met. **21**, 241 (1987).

[60] J. Obrzut and F. E. Karasz, J. Chem. Phys. **87**, 6178 (1987).

[61] D. D. C. Bradley, G. P. Evans, and R. H. Friend, Synth. Met. **17**, 651 (1987).

[62] A. Sakamoto, Y. Furukawa, and M. Tasumi, J. Phys. Chem. **98**, 4635 (1994).

[63] J. Fink *et al.*, in *Electronic Properties of Conjuigated Polymers*, edited by H. Kuzmany, M. Mehring, and S. Roth, Springer Series in Solid State Science Vol. 76 (Springer, Berlin, 1987), p. 79.

[64] A. Pron, F. Genoud, M. Nechtschein, and A. Rousseau, Synth. Met. **31**, 147 (1989).

[65] F. Genoud, M. Guglielmi, M. Nechtschein, E. Genies, and M. Salmon, Phys. Rev. Lett. **55**, 118 (1985).

[66] G. Froyer, Y. Pelous, A. Siove, F. Genoud, M. Nechtschein, and B. Villeret, Synth. Met. **33**, 381 (1989).

[67] M. Nechtschein, F. Devreux, F. Genoud, E. Vieil, J. M. Pernaut, and E. Genies, Synth. Met. **15**, 59 (1986).

[68] M. N. Bussac and L. Zuppiroli, Phys. Rev. B **47**, 5493 (1993).

[69] I. Orion, Ph.D. thesis, l'Université de Nantes, 1994.

[70] P. Bernier *et al.*, in *Electronic Properties of Polymers III*, edited by H. Kuzmany, M. Mehring, and S. Roth, Springer Series in Solid State Science Vol. 91 (Springer, Berlin, 1989), p. 193.

[71] Y. H. Kim, M. J. Winokur, and F. E. Karasz, Synth. Met. **55/1**, 509 (1993).

[72] M. Baitoul, J. P. Buisson, S. Lefrant, B. Dulieu, J. Wery, and M. Lapkowski, Synth. Met. **84**, 623 (1997).

[73] B. Tian, G. Zerbi, and K. Müllen, J. Chem. Phys. **95**, 3198 (1991).

[74] J. L. Brédas, R. R. Chance, and R. Silbey, Phys. Rev. B **26**, 5843 (1982).

[75] J. L. Brédas, B. Thémans, J. G. Fripiat, J. M. André, and R. R. Chance, Phys. Rev. B **29**, 6761 (1984).

[76] D. Emin, Phys. Rev. B **33**, 3973 (1986).

[77] H. A. Mizes and E. M. Conwell, Phys. Rev. Lett. **70**, 1505 (1993).